Metabolism 149 (2023) 155706

Contents lists available at ScienceDirect

Metabolism

journal homepage: www.journals.elsevier.com/metabolism

Angiotensin II type 1 receptor-associated protein in immune cells: a possible key factor in the pathogenesis of visceral obesity

Shunichiro Tsukamoto [a,1], Toru Suzuki [a,1], Hiromichi Wakui [a,*], Tatsuki Uehara [a], Juri Ichikawa [b], Hiroshi Okuda [b], Kotaro Haruhara [a,c], Kengo Azushima [a], Eriko Abe [a], Shohei Tanaka [a], Shinya Taguchi [a], Keigo Hirota [a], Sho Kinguchi [a], Akio Yamashita [d], Tomohiko Tamura [b,e], Kouichi Tamura [a,*]

[a] Department of Medical Science and Cardiorenal Medicine, Yokohama City University Graduate School of Medicine, Yokohama, Japan
[b] Department of Immunology, Yokohama City University Graduate School of Medicine, Yokohama, Kanagawa, Japan
[c] Division of Nephrology and Hypertension, Department of Internal Medicine, The Jikei University School of Medicine, Tokyo, Japan
[d] Department of Investigative Medicine Graduate School of Medicine, University of the Ryukyus, Okinawa, Japan
[e] Advanced Medical Research Center, Yokohama City University, Japan

ARTICLE INFO

Keywords:
Adipose tissue
Immune cell
Macrophage
Metabolic disorders
Receptor signaling
Visceral obesity

ABSTRACT

Background and aim: Dysregulation of angiotensin II type 1 receptor-associated protein (ATRAP) expression in cardiovascular, kidney, and adipose tissues is involved in the pathology of hypertension, cardiac hypertrophy, atherosclerosis, kidney injury, and metabolic disorders. Furthermore, ATRAP is highly expressed in bone marrow-derived immune cells; however, the functional role of immune cell ATRAP in obesity-related pathology remains unclear. Thus, we sought to identify the pathophysiological significance of immune cell ATRAP in the development of visceral obesity and obesity-related metabolic disorders using a mouse model of diet-induced obesity.

Methods: Initially, we examined the effect of high-fat diet (HFD)-induced obesity on the expression of immune cell ATRAP in wild-type mice. Subsequently, we conducted bone marrow transplantation to generate two types of chimeric mice: bone marrow wild-type chimeric (BM-WT) and bone marrow ATRAP knockout chimeric (BM-KO) mice. These chimeric mice were provided an HFD to induce visceral obesity, and then the effects of immune cell ATRAP deficiency on physiological parameters and adipose tissue in the chimeric mice were investigated.

Results: In wild-type mice, body weight increase by HFD was associated with increased expression of immune cell ATRAP. In the bone marrow transplantation experiments, BM-KO mice exhibited amelioration of HFD-induced weight gain and visceral fat expansion with small adipocytes compared BM-WT mice. In addition, BM-KO mice on the HFD showed significant improvements in white adipose tissue metabolism, inflammation, glucose tolerance, and insulin resistance, compared with BM-WT mice on the HFD. Detailed analysis of white adipose tissue revealed significant suppression of HFD-induced activation of transforming growth factor-beta signaling, a key contributor to visceral obesity, via amelioration of $CD206^{+}$ macrophage accumulation in the adipose tissue of BM-KO mice. This finding suggests a relevant mechanism for the anti-obesity phenotype in BM-KO mice on the HFD. Finally, transcriptome analysis of monocytes indicated the possibility of genetic changes, such as the enhancement of interferon-γ response at the monocyte level, affecting macrophage differentiation in BM-KO mice.

Abbreviations: ATRAP, angiotensin II type 1 receptor-associated protein; ATM, adipose tissue macrophages; BM-WT, bone marrow wild-type chimeric; BM-KO, bone marrow ATRAP knockout chimeric; BW, Body weight; CEBP-α, CCAAT/enhancer-binding protein-α; CTL, control diet; DEG, differentially expressed gene; eWAT, epididymal white adipose tissue; GLUT-4, glucose transporter type 4; GSEA, gene set enrichment analysis; GTT, glucose tolerance test; HFD, high-fat diet; IL, Interleukin; ITT, insulin tolerance test; MCP-1, monocyte chemoattractant protein-1; PCR, polymerase chain reaction; PGC1-α, proliferator-activated receptor gamma coactivator 1-α; TGF-β, transforming growth factor-β 1; TNF-α, tumor necrosis factor-α; UCP-1, uncoupling protein-1; WAT, white adipose tissue.

* Corresponding authors at: Department of Medical Science and Cardiorenal Medicine, Yokohama City University Graduate School of Medicine, 3-9 Fukuura, Kanazawa-ku, Yokohama 236-0004, Japan.
E-mail address: hiro1234@yokohama-cu.ac.jp (H. Wakui).
[1] These authors contributed equally to this work.

https://doi.org/10.1016/j.metabol.2023.155706
Received 5 June 2023; Accepted 9 October 2023
Available online 13 October 2023

Conclusion: Collectively, our results indicate that ATRAP in bone marrow-derived immune cells plays a role in the pathogenesis of visceral obesity. The regulation of ATRAP expression in immune cells may be a key factor against visceral adipose obesity with metabolic disorders.

1. Introduction

The global prevalence of obesity has increased, almost threefold, between 1975 and 2016. By 2035, approximately 2 billion people, or 24 % of the world's population, are expected to be obese [1,2]. Additionally, visceral obesity is a highly probable comorbidity for various diseases, including cardiovascular disease, diabetes, chronic kidney disease, and cancer, and is associated with an increased risk of these diseases [3–6]. Addressing the increasing prevalence of obesity is an urgent public health issue.

In the pathogenesis of obesity, the accumulation of excess energy is modulated by the augmentation of white adipose tissue (WAT) [7,8]. Continued energy overload increases the number of lipids stored by adipocytes, causing an enlargement of adipocytes and expansion of WAT [7,8]. Despite the involvement of various bone marrow-derived immune cells, including macrophages, in the remodeling process of WAT [9–11], numerous mechanisms underlying the relationship between the pathophysiology of obesity and immune cells remain unexplored. Investigating the effects of alterations in gene expression in immune cells on the pathogenesis of obesity may lead to the elucidation of its pathophysiological basis and novel therapeutic strategies.

Angiotensin II type 1 receptor-associated protein (ATRAP) was identified as a molecule interacting directly with the angiotensin II type 1 receptor [12]. In a previous study, we showed that ATRAP is expressed in cardiovascular, kidney, and adipose tissues and that dysregulation of ATRAP expression in these tissues is involved in the pathology of hypertension, cardiac hypertrophy, atherosclerosis, kidney injury, and metabolic disorders [13–16]. In our previous study using systemic ATRAP knockout (ATRAP-KO) mice, ATRAP deficiency exacerbated diabetic kidney injury through decreased number of M2 ($CD206^{+}$) macrophages in the kidney [13]. In addition, deficiency of bone marrow ATRAP has been found to be associated with lipopolysaccharide-induced leukocyte inflammation [17]. ATRAP is abundantly expressed in bone marrow-derived immune cells such as granulocytes and monocytes in mice and humans; in patients with chronic non-infectious diseases, leukocyte ATRAP is associated with the inflammatory status of these patients [17]. The results of these studies suggest that immune cell ATRAP plays a role in macrophage polarization and influences systemic inflammatory status [13,17]. However, the functional role of immune cell ATRAP in obesity-related pathology is unclear. Thus, the present study was conducted to elucidate the pathophysiological importance of immune cell ATRAP in the development of visceral obesity using a mouse model of high-fat diet (HFD)-induced obesity.

2. Materials and methods

2.1. Animal experiments

This study was performed following the National Institutes of Health guidelines for using experimental animals. It was reviewed and approved by the Animal Studies Committee of Yokohama City University. Male C57BL/6 wild-type (WT) mice were purchased from Charles River Laboratories (Wilmington, MA, USA). We used systemic ATRAP-KO mice in a C57BL/6 background, which had been generated using a targeted gene disruption strategy, as described previously [13,16–18]. The mice were housed in a controlled environment with a 12-h light/dark cycle at 25 °C and were allowed free access to food and water.

2.2. Generation of bone marrow chimeric mice and dietary high fat loading to induce visceral obesity

First, 8-week-old male C57BL/6 WT mice were divided into control diet and HFD groups, fed for 3 weeks, and then sacrificed and analyzed. Next, recipient 8-week-old male WT mice were lethally irradiated with 9.5 Gy. Bone marrow cells were harvested by flushing the femurs and tibias of donor WT and ATRAP-KO mice. Within 24 h after irradiation, the recipient mice were injected through the tail vein with 1×10^6 bone marrow cells suspended in 0.4 mL of RPMI 1640 (Nacalai Tesque, Kyoto, Japan) from WT or ATRAP-KO mouse donors. Polymerase chain reaction (PCR) was used to confirm the bone marrow genotype by examining the ATRAP gene expression in circulating immune cells. Six weeks after bone marrow transplantation, the mice were divided into control diet and HFD groups; they were fed either a control diet (3.6 kcal/g; 13.3 % energy as fat; Oriental Yeast Co, Ltd., Tokyo, Japan) or an HFD diet (5.6 kcal/g; 60.0 % energy as fat) for 8 weeks, and their body weight (BW) and food intake were measured weekly. CD45.1 (Ly5.1) mice were the recipients for the macrophage flow cytometry experiments. Ly5.1 congenic mice were purchased from Sankyo Labo Service Corporation (Tokyo, Japan). Recipient Ly5.1 WT mice were lethally irradiated with 9.5 Gy. Bone marrow cells were harvested by flushing the femurs and tibias of donor CD45.2 (Ly5.2) WT and Ly5.2 ATRAP-KO mice. Other procedures were repeated in the same manner.

2.3. Glucose and insulin tolerance tests

The glucose tolerance test (GTT) and insulin tolerance test (ITT) were conducted via intraperitoneal injection of standard doses of glucose or insulin, respectively [15,19]. Details are described in the supplemental materials. K_{ITT}, an index of insulin sensitivity, was calculated from the formula $K_{ITT} = 0.693 / t1/2$ based on the rate of glucose disappearance [20]. Plasma glucose *t1/2* was calculated from the slope of plasma glucose concentration from 0 to 15 min after bolus injection of insulin. Homeostasis model assessment of insulin resistance (HOMA-IR) was calculated from the following equation, HOMA-IR = insulin (μu/ml) / $22.5\ e^{-\ln \text{ glucose (mmol/L)}}$ [21].

2.4. Histological analyses

Epididymal WAT (eWAT) was collected and fixed with 10 % paraformaldehyde overnight and embedded in paraffin. Details are described in the supplemental materials.

2.5. Real-time quantitative reverse transcription PCR analysis

Total leukocyte RNA was extracted using the PAX gene Blood RNA Kit (QIAGEN, Hilden, Germany) for reverse transcription. Total eWAT RNA was extracted using ISOGEN (Nippon Gene, Tokyo, Japan), and total immune cell, monocyte, neutrophil, T cell, B cell, and adipose tissue macrophage [ATM] RNA was extracted using RNeasy micro kit (QIAGEN). Complementary DNA was synthesized using the SuperScript III First-Strand System (Invitrogen, Carlsbad, CA, USA), as described previously [22]. Real-time quantitative reverse transcription PCR analysis was performed using the ABI PRISM 7000 Sequence Detection System by incubating the reverse transcription products with the TaqMan PCR Master Mix and TaqMan probes (Applied Biosystems, Foster City, CA, USA). The TaqMan probes used for PCR are shown in the supplementary materials. mRNA levels were normalized to 18S rRNA level.

2.6. Western blotting

Protein expression was analyzed using western blotting of tissue homogenates, as described previously [22]. Details are provided in the supplementary materials. Briefly, equal amounts of extracted protein extract were separated using 5 %–20 % sodium dodecyl sulfate–polyacrylamide gel electrophoresis and transferred onto a polyvinylidene difluoride membrane using the iBlot Dry Blotting System (Invitrogen, Paisley, UK). The membranes were blocked with 1 % bovine serum albumin and probed with specific primary antibodies, and horseradish peroxidase-conjugated goat anti-rabbit IgG secondary antibodies were added. The images were captured with auto-exposure, and automatically optimized using ChemiDoc Touch (Bio-Rad Laboratories).

2.7. Measurement of blood hormones

Whole blood samples were centrifuged at 3000 rpm (MR-150; Tomy Seiko Co., Ltd., Tokyo, Japan) at 4 °C for 10 min to separate the plasma. Plasma insulin concentration was measured using mouse insulin (Morinaga Institute of Biological Science) ELISA kits.

2.8. Cell isolation and flow cytometric analysis

Excised eWAT was minced and homogenized using a 70-μm cell strainer (Corning Life Sciences, Corning, NY, USA). The cells were resuspended in RPMI 1640 solution containing 10 % fetal bovine serum and centrifuged at 300 ×*g* for 10 min to concentrate the fat-infiltrating immune cells and then treated with red blood cell lysate. Circulating immune cells were obtained by treating peripheral blood twice with erythrocyte lysate. The cells were incubated for 30 min at 4 °C for surface marker staining with appropriately diluted antibodies. ATMs were fractionated using APC/Cy7-anti-CD11c and PE-anti-CD206 (Biolegend, San Diego, CA, USA) after separation with BV605-anti-CD11b and APC-anti-F4/80 (Biolegend), respectively. Neutrophils and monocytes were fractionated using APC/Cy7-anti-Ly6G and BV605-anti-CD115 (Biolegend), respectively, after separation with BV711-anti-CD11b (Biolegend). B and T lymphocytes were fractionated using PE/Cy7-anti-CD45R and FITC-anti-CD 3ε (Biolegend), respectively. Flow cytometry was performed using FACSAria II (BD Biosciences, Franklin Lakes, NJ, USA), and data were analyzed using FlowJo software (FlowJo, Ashland, OR, USA).

2.9. RNA sequencing

2.9.1. Library preparation and RNA sequencing

Total RNA was prepared using the RNeasy Micro kit (QIAGEN). Complimentary DNA was synthesized and amplified using the SMART-Seq v4 Ultra Low Input RNA Kit for Sequencing (Clontech, Mountain View, CA, USA). RNA sequencing (RNA-seq) libraries were prepared using the Nextera XT kit (Illumina, San Diego, CA, USA). Single-end 75 bp sequencing was conducted on the NextSeq 500 platform (Illumina).

2.9.2. Data analysis

Following the GitHub RNA-seq pipeline riboduct (https://github.com/msfuji/riboduct), sequencing reads were aligned to a mouse reference genome (UCSCmm10) in STAR software (version 2.7.4a). FeatureCounts (v2.0.0) was used to quantify the transcripts of the aligned reads using the corresponding UCSCmm10 gene annotation model. The generated count data were input for differential gene analysis using EdgeR (EdgeR version 3.40.0 and R version 4.1.0). Quantile methods were used to normalize all TPM data.

2.9.3. Gene set enrichment analysis

Normalized RNA-seq data from monocyte populations served as expression datasets. Gene Set Enrichment Analysis (GSEA) was performed in fgsea (fgsea version 1.18.0 and R version 4.1.0) [23].

2.10. Statistical analysis

Statistical analyses were performed using Prism software version 9 (GraphPad Software, San Diego, CA, USA). All data are expressed as mean ± standard error. The differences were analyzed as follows. A two-way repeated-measures analysis of variance with Tukey's post-hoc analysis was performed to determine differences over time between groups (Figs. 1A, 2B, D, 3A, B). A two-way factorial analysis of variance with Tukey's post-hoc analysis was used to determine the differences in the same diet within each genotype or differences in the WT versus knockout mice (Figs. 2C, E, 4B–G, 5A–E, 6A, C, F, 7B–G, 8A–C). An unpaired *t*-test was used to determine the differences between groups (Fig. 1B–E, G, H). For all unpaired *t*-tests conducted in this study, normality was confirmed using Shapiro–Wilk and Kolmogorov–Smirnov tests. Statistical significance was set at $p < 0.05$.

3. Results

3.1. Leukocyte ATRAP gene expression was upregulated in HFD-induced obesity

Initially, we examined whether the development of diet-induced obesity affected ATRAP expression in immune cells using leukocytes derived from male WT mice fed an HFD for 3 weeks. ATRAP mRNA expression was significantly increased in leukocytes, concomitant with BW gain, starting from the early phase of obesity (Fig. 1-A, B). A small increase in visceral fat weight and adipocyte size was also observed in HFD mice (Fig. 1-C, D, E). In addition, abundant macrophage infiltrates were already observed in HFD mice (Fig. 1-F, G).

3.2. Deletion of bone marrow ATRAP ameliorated HFD-induced weight gain and visceral fat growth

Next, bone marrow ATRAP knockout chimeric (BM-KO) mice and bone marrow WT chimeric (BM-WT) mice were generated to investigate the functional role of immune cell ATRAP in the development of visceral obesity. Six weeks after bone marrow transplantation, ATRAP expression was almost absent in the circulating immune cells of BM-KO mice (Fig. S1). In addition, ATRAP expression in circulating immune cells of BM-WT mice was the highest in monocytes (Fig. S1). BM-KO and BM-WT mice were fed either an HFD or control diet for 8 weeks (Fig. 2A). After 8 weeks, there was no significant difference in BW between BM-WT mice fed a control diet (BM-WT/CTL), and BM-KO mice fed a control diet (BM-KO/CTL). The HFD groups showed significant BW gain compared with the control diet groups; however, the BW of BM-KO mice fed an HFD (BM-KO/HFD) significantly decreased compared with that of BM-WT mice fed an HFD (BM-WT/HFD) (Fig. 2B). Similarly, the eWAT weight of BM-KO/HFD mice was significantly lower than that of BM-WT/HFD mice (Fig. 2C). The two genotypes showed no significant difference in caloric intake (Fig. 2D, E).

3.3. Deletion of bone marrow ATRAP ameliorated metabolic disorder

The apparent improvement in visceral fat weight gain in BM-KO/HFD mice prompted us to investigate whether diet-induced insulin resistance is improved in BM-KO/HFD mice. The non-fasting insulin levels were significantly increased by HFD in BM-WT mice, but not in BM-KO mice (Table S1). We performed GTT and ITT, reflecting glucose tolerance and insulin sensitivity, respectively. In GTT, glucose tolerance was significantly improved in BM-KO/HFD mice compared with BM-WT/HFD mice (Fig. 3A). In ITT, although the curves of the BM-WT/HFD and BM-KO/HFD mice were statistically different, the difference in slope was small (Fig. 3B). However, the K_{ITT}, which evaluates insulin sensitivity based on the rate of glucose disappearance, showed

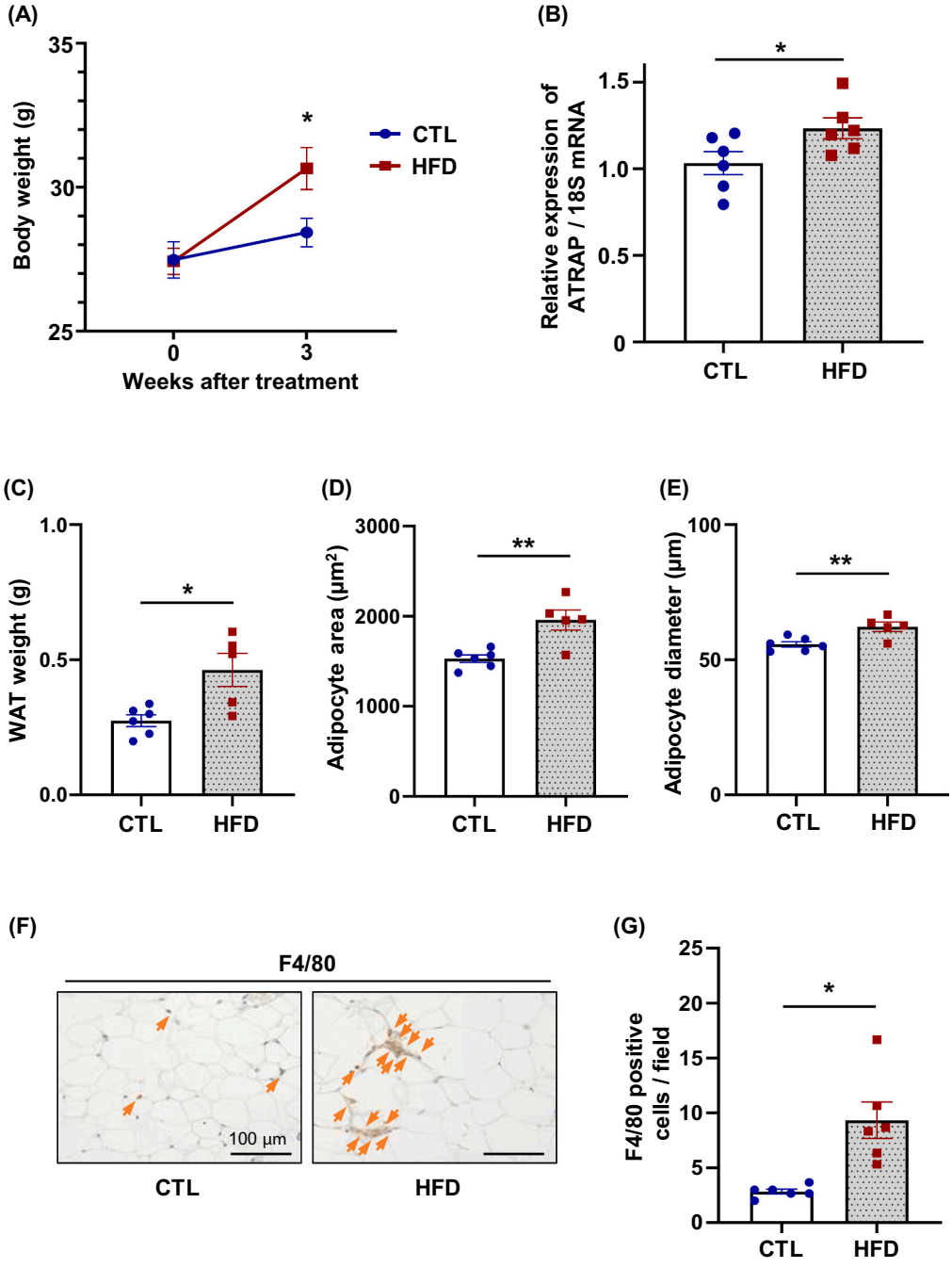

Fig. 1. Effects of an HFD on body weight and the expression of leucocyte ATRAP in wild-type mice.
(A) The change in body weight in wild-type mice fed a CTL or an HFD. (B) Relative mRNA expression of ATRAP in leucocytes. (C) WAT weight, (D) adipocyte area, and (E) diameter of WAT. (F) Representative images of WAT stained with anti-F4/80 antibody (bars = 50 μm) and (G) the number of F4/80-positive cells in WAT. Values are expressed as mean ± standard error (n = 4 to 6). *$p < 0.05$, **$p < 0.01$ vs. control diet group. CTL, control diet; HFD, high-fat diet.

significant improvement in BM-KO/HFD mice compared with BM-WT/HFD mice (Fig. 3C). Fasting insulin levels and HOMA-IR were also lower in BM-KO/HFD mice than those in BM-WT/HFD mice, indicating that insulin sensitivity was improved in BM-KO/HFD mice compared with BM-WT/HFD mice (Fig. 3D, E).

3.4. Deletion of bone marrow ATRAP ameliorated HFD-induced adipocyte enlargement and upregulated metabolically favorable gene expression in WAT

Adipose tissue physiology was assessed by analyzing adipocyte size and number. There was no difference in adipocyte size in eWAT between BM-WT/CTL and BM-KO/CTL mice (Fig. 4A, B, C). The size of adipocytes in eWAT was significantly reduced in BM-KO/HFD mice compared with that in BM-WT/HFD mice (Fig. 4A, B, C). In contrast, the number of adipocytes increased in BM-KO/HFD mice (Fig. 4D). Gene expression analysis of eWAT showed that the level of glucose transporter type 4 (GLUT-4), involved in glucose uptake, was significantly increased in BM-KO/HFD mice compared with that in BM-WT/HFD mice (Fig. 4E), and the expression of proliferator-activated receptor gamma coactivator 1-α (PGC1-α), involved in energy production, was not decreased by the HFD in BM-KO mice (Fig. 4F). The expression of uncoupling protein-1 (UCP-1), involved in heat production mainly in brown adipose tissue, was also significantly increased in BM-KO/HFD mice compared with that in BM-

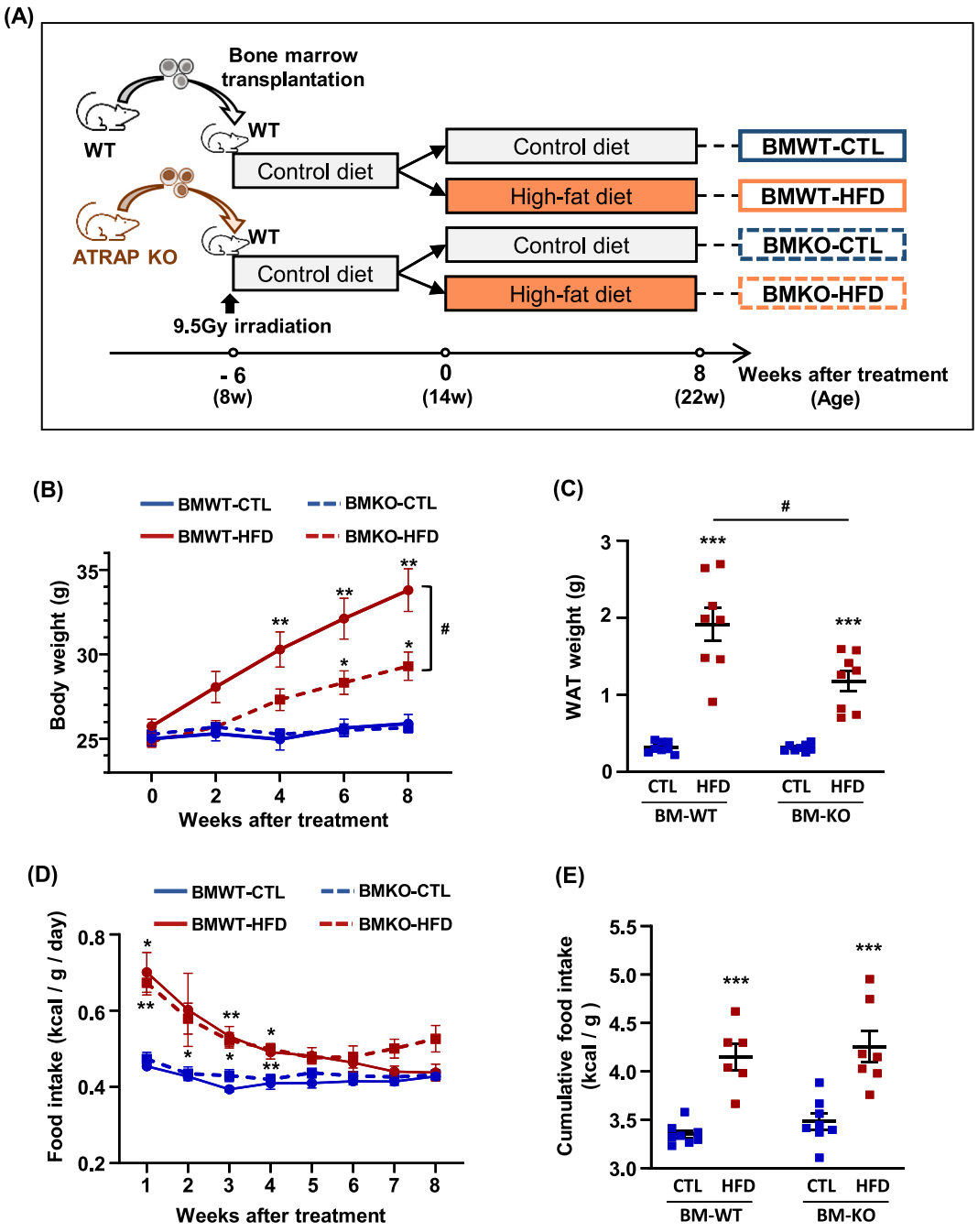

Fig. 2. Effect of bone marrow ATRAP deficiency on HFD-Induced obesity.
(A) Experimental protocol (see Methods for details). (B) The change in body weight in BM-WT mice and BM-KO mice fed a CTL or an HFD. (C) The difference in WAT weight in BM-WT mice and BM-KO mice fed a CTL or an HFD. (D) Caloric intake per body weight (gram) during the experimental period. (E) Cumulative caloric intake per body weight (gram) during the experimental period. Values are expressed as mean ± standard error (n = 6 to 8). $^{*}p < 0.05$, $^{**}p < 0.01$, $^{***}p < 0.001$ vs. control diet group. $^{\#}p < 0.05$, $^{\#\#}p < 0.01$ vs. BM-WT group. CTL, control diet; HFD, high-fat diet; BM-WT mice, bone marrow wild-type chimeric mice; BM-KO mice, bone marrow ATRAP-deficient chimeric mice.

WT/HFD mice (Fig. 4G). Furthermore, the protein expression of GLUT-4, PGC1-α, and UCP-1 was higher or tended to be higher in the adipose tissue of BM-KO/HFD mice than in the adipose tissue of BM-WT/HFD mice (Fig. 4H). In BM-KO/HFD mice, the expression of cell cycle-related-, adipose-derived stem cell related-, and adipogenesis related-genes, such as cyclin B1, Ly6a, and CCAAT/enhancer-binding protein-α (CEBP-α), increased significantly or trend to increase compared with that in BM-WT/HFD mice (Fig. S2). These changes in gene expression in adipose tissue may reflect the smaller size, greater number, and favorable metabolic status of adipocytes in BM-KO/HFD mice.

3.5. Deletion of bone marrow ATRAP ameliorated HFD-induced activation of TGF-β signaling in WAT

Transforming growth factor-beta 1 (TGF-β) and its downstream signaling (p-15, p-16, p-21) in eWAT were investigated to identify the underlying factors contributing to the differences in adipocyte hypertrophy, adipocyte number, and adipose tissue metabolism between BM-KO/HFD and BM-WT/HFD mice observed in the present study. TGF-β signaling was reportedly associated with adipocyte differentiation and obesity development, and inhibiting this pathway reduced the size of

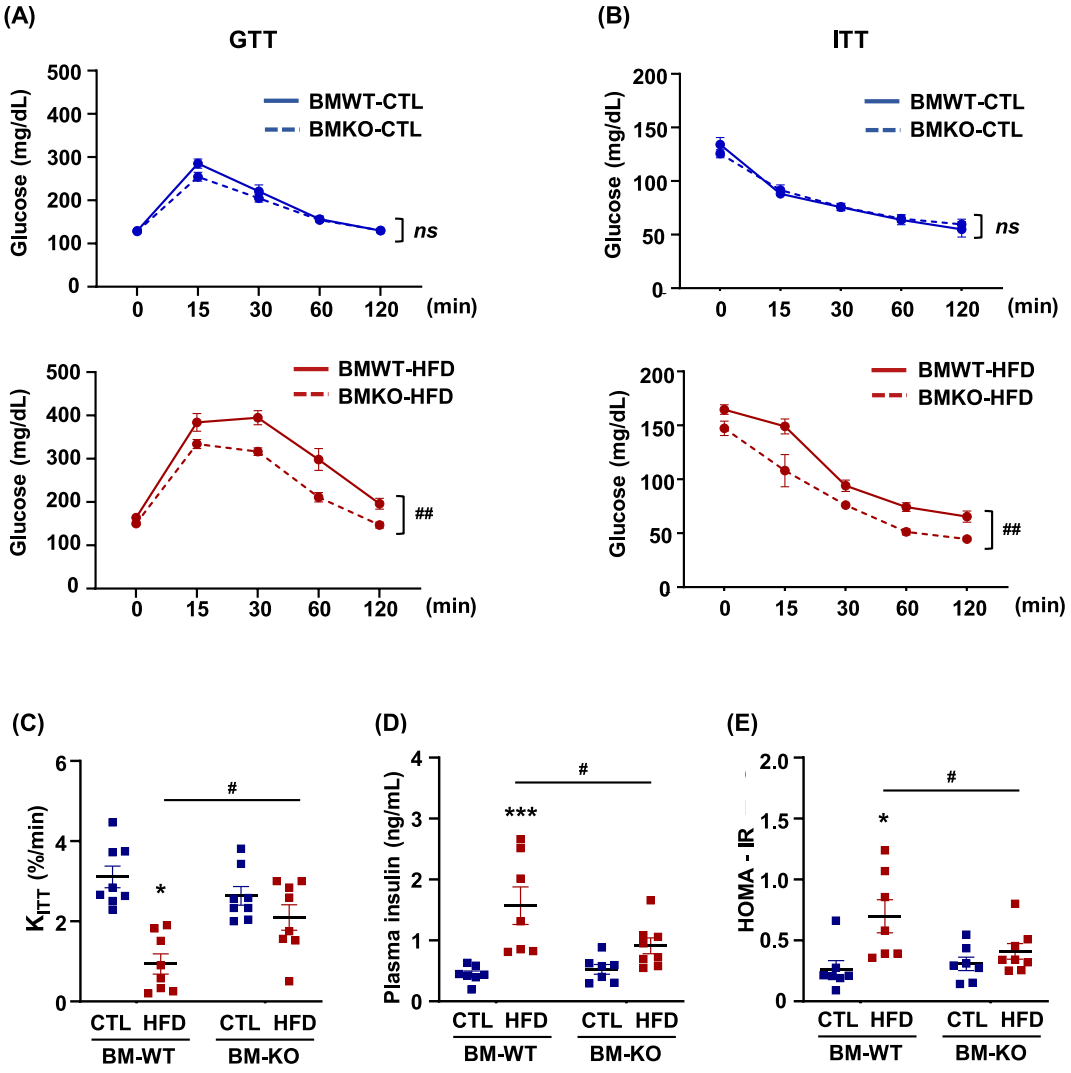

Fig. 3. GTT and ITT in BM-WT and BM-KO mice.
(A) GTT and (B) ITT in the BM-WT and BM-KO mice after 8 weeks of CTL or HFD feeding. (C) K_{ITT}, (D) fasting plasma insulin, and (E) HOMA-IR in the BM-WT and BM-KO mice fed an HFD. Values are expressed as mean ± standard error (n = 6 to 8). $^{*}p < 0.05$, $^{***}p < 0.001$ vs. control diet group; $^{\#}p < 0.05$, $^{\#\#}p < 0.01$ vs. BM-WT group. CTL, control diet; HFD, high-fat diet; BM-WT mice, bone marrow wild-type chimeric mice; BM-KO mice, bone marrow ATRAP-deficient chimeric mice.

adipocytes [10,24]. In the HFD group, TGF-β gene expression was significantly decreased in eWAT of BM-KO/HFD mice compared with that in BM-WT/HFD mice (Fig. 5A). Furthermore, the expression of TGF-β downstream genes (p-15, p-16, and p-21) and Interleukin (IL)-10 significantly decreased or showed a decreasing trend in BM-KO/HFD mice (Fig. 5B, C, D, E). Histological findings also showed a decrease in the number of TGF-β-positive cells in eWAT of BM-KO/HFD mice compared with that in BM-WT/HFD mice (Fig. 5F). These findings suggest that the downregulation of these signaling pathways contributed to differences in adipocyte differentiation/proliferation and hypertrophy between BM-KO/HFD and BM-WT/HFD mice observed in the present study.

3.6. Amelioration of HFD-induced accumulation of adipose tissue $CD206^{+}$ macrophages in BM-KO mice

Next, to identify the mechanism responsible for the reduced TGF-β signaling and IL-10 expression in BM-KO/HFD mice, we analyzed the ATM population in eWAT. The expression of F4/80 mRNA in eWAT was significantly decreased in BM-KO/HFD mice compared with that in BM-WT/HFD mice (Fig. 6A). In addition, immunohistochemical analysis of F4/80 revealed a pronounced enhancement of macrophage infiltration in BM-WT/HFD mice, but not in BM-KO/HFD mice (Fig. 6B, C). Flow cytometric analysis was performed to determine the frequency with which ATMs were replaced with those that were donor-derived. In this analysis, bone marrow was extracted from Ly5.2 WT or ATRAP-KO mice and was transplanted to Ly5.1 WT mice as recipients (Fig. S3). After 8 weeks of HFD feeding, approximately 95 % of ATMs ($F4/80^{+}/CD11b^{+}$) were replaced by donor-derived macrophages ($CD45.2^{+}$) (Figs. 6D, S4). Flow cytometry also revealed that the HFD failed to increase ATM count in BM-KO mice (Fig. 6E, F). We further fractionated these ATMs by CD11c and CD206 (Fig. 7A, B, C). The fluorescence intensity of CD206 in ATMs and the number of $CD206^{+}$ ATMs ($CD11c^{+}/CD206^{+}$ and $CD11c^{-}/CD206^{+}$) in eWAT were significantly reduced in BM-KO/HFD mice compared with those in BM-WT/HFD mice (Fig. 7C, D, E). The increase in the number of $CD11c^{+}$ ATMs by the HFD was inhibited in BM-KO mice (Fig. 7B, F); however, the number of double-negative ATMs ($CD11c^{-}/CD206^{-}$) did not differ between genotypes (Fig. 7G). We evaluated whether the shift in macrophage polarity in BM-KO/HFD mice is involved in the exacerbation of adipose tissue inflammation. The increase in mRNA expression of inflammation-related genes (monocyte chemoattractant protein-1 [MCP-1], tumor necrosis factor-α [TNF-α],

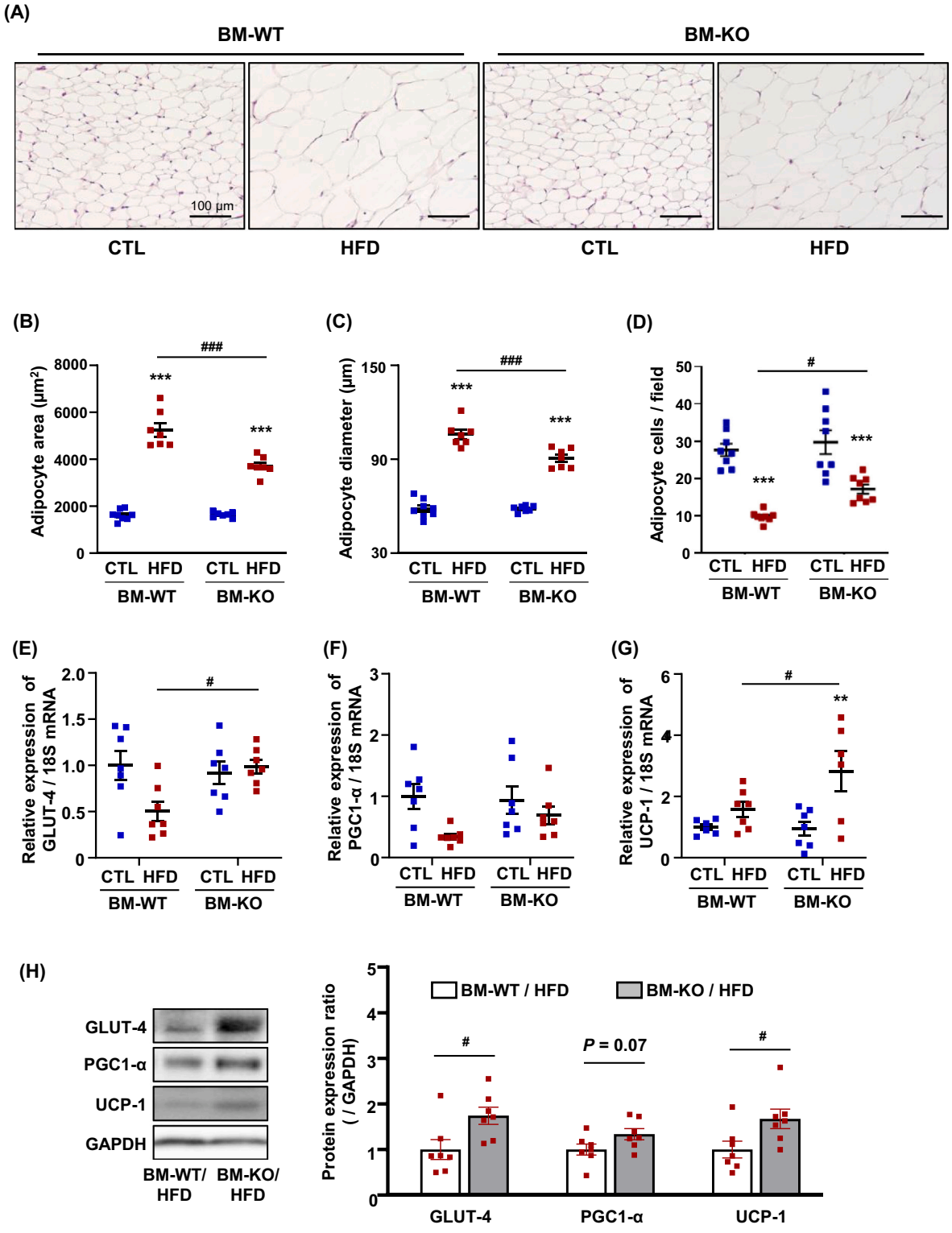

Fig. 4. Effect of bone marrow ATRAP deficiency on WAT in HFD-induced obesity.
(A) Representative images of WAT from BM-WT and BM-KO mice after 8 weeks of CTL or HFD feeding stained with hematoxylin and eosin (bars = 100 μm). (B) Adipocyte area, (C) diameter, and (D) number of WAT in BM-WT and BM-KO mice. (E–G) Relative mRNA expression of GLUT-4, PGC1-α, and UCP-1 in WAT. (H) Relative protein expression level (GLUT-4, PGC1-α, and UCP-1 / GAPDH) in WAT. Values are expressed as mean ± standard error (n = 6 to 7). $^{*}p < 0.05$, $^{**}p < 0.01$, $^{***}p < 0.001$ vs. control diet group; $^{\#}p < 0.05$, $^{\#\#\#}p < 0.001$ vs. BM-WT group. CTL, control diet; HFD, high-fat diet; BM-WT mice, bone marrow wild-type chimeric mice; BM-KO mice, bone marrow ATRAP-deficient chimeric mice.

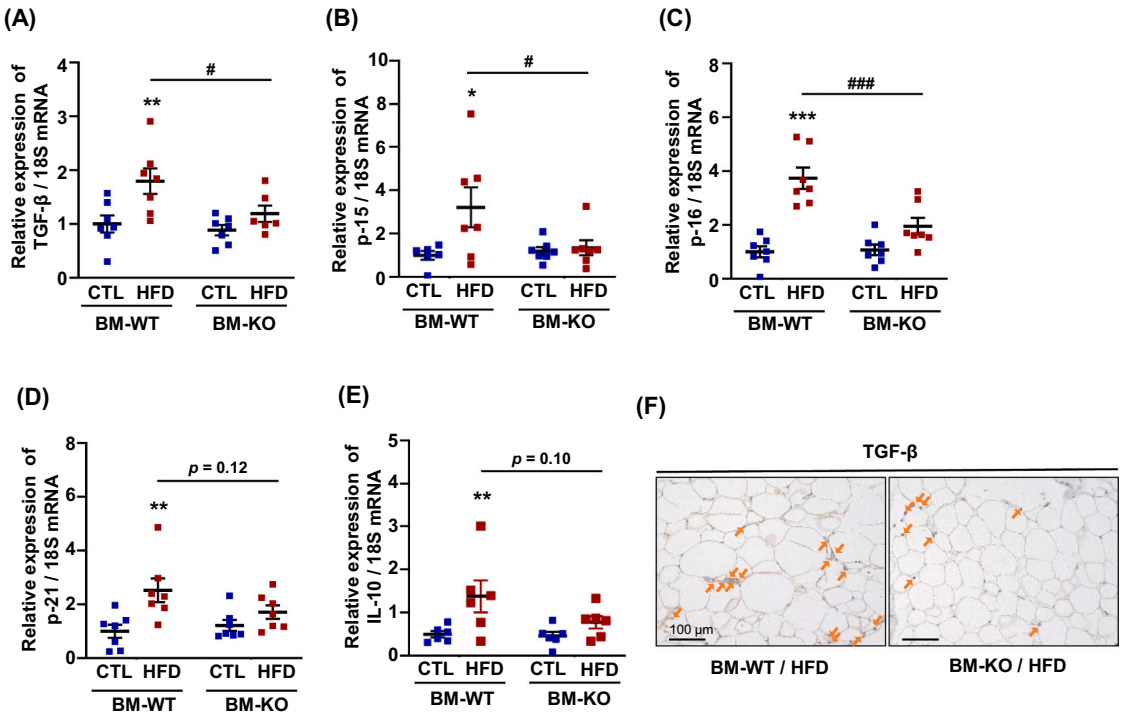

Fig. 5. Effects of bone marrow ATRAP deficiency on TGF-β related signaling in obese WAT.
(A–E) Relative mRNA expression of TGF-β, p-15, p-16, p-21, and IL-10 in WAT. (F) Representative images of WAT from BM-WT and BM-KO mice after 8 weeks of CTL or HFD feeding stained with anti-TGF-β antibody (bars = 100 μm). Values are expressed as mean ± standard error (n = 6 to 7). $^{*}p < 0.05$, $^{**}p < 0.01$, $^{***}p < 0.001$ vs. control diet group; $^{\#}p < 0.05$, $^{\#\#\#}p < 0.001$ vs. BM-WT group. CTL, control diet; HFD, high-fat diet; BM-WT mice, bone marrow wild-type chimeric mice; BM-KO mice, bone marrow ATRAP-deficient chimeric mice.

and IL-6) by the HFD was suppressed in eWAT of BM-KO/HFD mice (Fig. 8A, B, C).

3.7. Monocytes from BM-KO mice exhibited genetic modifications preventing polarization to adipose tissue CD206^{+} macrophages

We performed RNA sequencing of monocytes to investigate the mechanism of reduced CD206^{+} ATMs in eWAT of BM-KO/HFD mice. Differentially expressed genes (DEGs) were identified using filtering characteristics, with fold change >2 ($p < 0.05$). A total of 407 genes in the control diet group and 323 genes in the HFD group were identified as differentially expressed between BM-WT and BM-KO mice. Heat maps and principal component analysis plots for each group are shown in Fig. 9A and B. The top 20 up/downregulated DEGs between BM-WT and BM-KO mice are listed in the supplementary material (Fig. S5). Among the groups of genes with significant expression changes between BM-WT and BM-KO, in both control diet and HFD groups, the volcano plot revealed that monocytes from BM-KO mice showed downregulation of genes that may promote polarization to CD206^{+} macrophages and TGF-β signaling (Thbs1, Nr4a2, and Loxl4) [25–27] and upregulation of genes that may suppress polarization to CD206^{+} macrophages and TGF-β signaling (CXCR2, Htra3, Saa3, Wfdc21, Xrcc5, Lcn2, and S100a9) (Fig. 9C) [28–34]. In contrast, the expression of several genes with reported beneficial effects on obesity and metabolism was upregulated in BM-KO mice (LRG1 and S1pr3) [35,36] (Fig. 9C). The top six upregulated and downregulated pathways from the GSEA of each group are shown in Fig. 9D. The GSEA revealed that in HFD-fed mice, inflammation-related pathways, such as interferon-γ response, were enhanced in BM-KO mice.

4. Discussion

The present study demonstrated that the expression of bone marrow-derived immune cell ATRAP, predominantly in monocytes, was increased by the development of visceral obesity. Conversely, bone marrow ATRAP deletion ameliorated HFD-induced obesity and visceral fat gain. Moreover, the infiltration of HFD-induced adipose tissue macrophage, especially CD206^{+} macrophages, was significantly suppressed in BM-KO mice compared with that in BM-WT mice, along with inhibition of TGF-β signaling and IL-10 gene expression in adipose tissue (Fig. 10). These alterations in the adipose tissue environment may have contributed to the amelioration of visceral obesity and adipose hypertrophy and inflammation, the increase in adipocyte number and the improvements in adipose tissue metabolism, as well as insulin resistance and glucose tolerance, which are characteristic features of visceral obesity. RNA-seq revealed that monocytes in BM-KO mice undergo genetic changes that could possibly attenuate the HFD-induced increase and polarity of CD206^{+} macrophages.

TGF-β regulates the development, growth, and function of diverse cell types via the induction of related factors such as the cyclin-dependent kinase inhibitors p15, p16, and p21 [24,37,38]. The suppression of TGF-β signaling and IL-10 expression reportedly improves obesity pathology [24,39]. Deletion of Smad3, located downstream of TGF-β signaling, or blockade of TGF-β by neutralizing antibodies, improves obesity and insulin resistance with a reduction in adipocyte size and browning of WAT [24]. As CD206^{+} ATMs enhance TGF-β signaling and IL-10 expression in adipose tissue, elimination or downregulation of CD206^{+} macrophages also reportedly improve obesity along with an increase in the number of smaller adipocytes, browning of WAT, and improved insulin sensitivity by regulating downstream signals such as TGF-β [10,40]. In the present study, the deletion of immune cell ATRAP suppressed the accumulation of CD206^{+} ATMs and reduced TGF-β signaling in WAT, suggesting that these mechanisms are associated with improving visceral obesity and metabolism in BM-KO/HFD mice.

A possible mechanism underlying the reduction of CD206^{+} ATMs, which are involved in the suppression of obesity onset and progression,

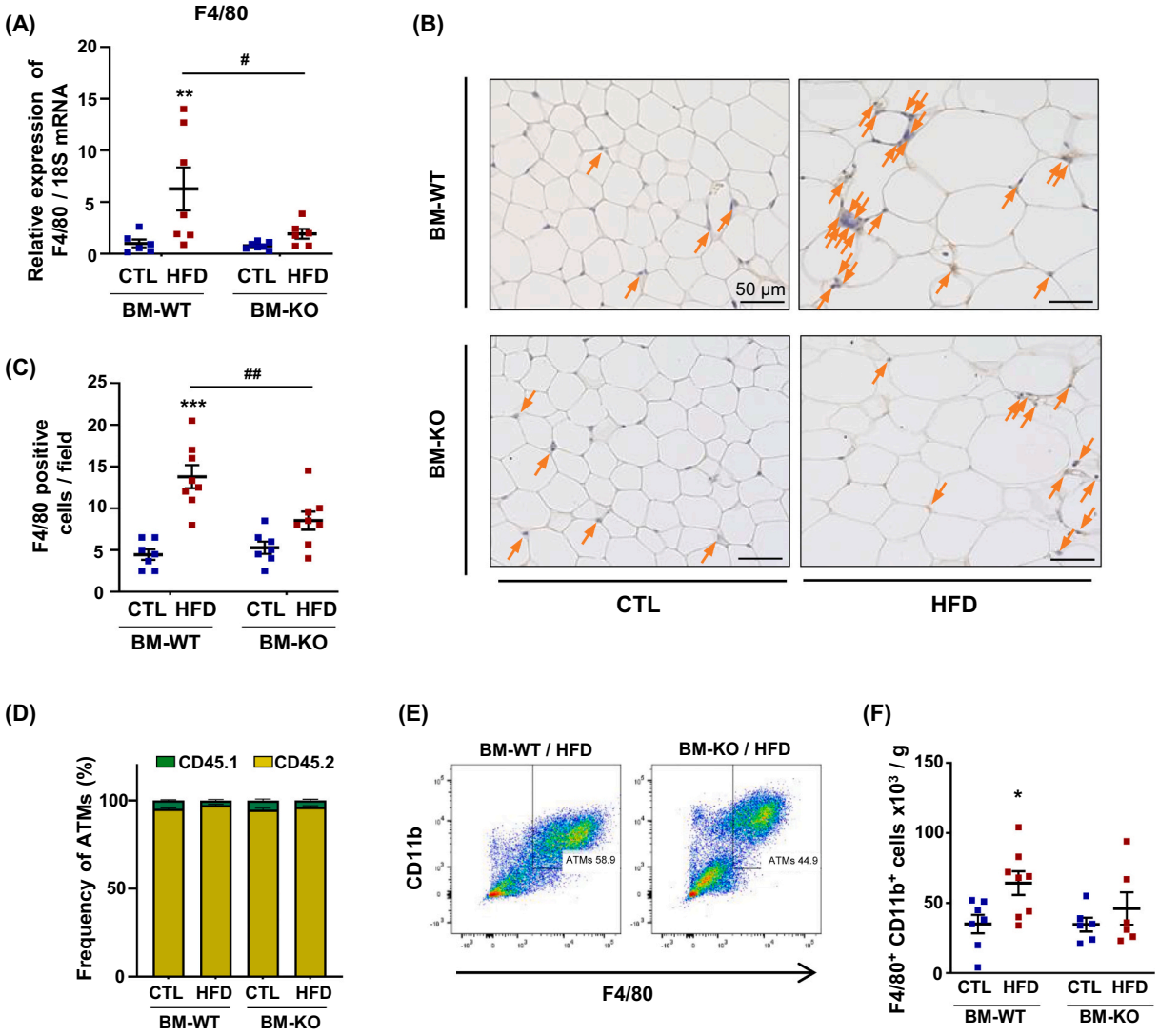

Fig. 6. Effect of bone marrow ATRAP deficiency on ATMs in HFD-induced obesity.
(A) Relative mRNA expression of F4/80 in WAT. (B) Representative images of WAT from BM-WT and BM-KO mice after 8 weeks of CTL or HFD feeding stained with anti-F4/80 antibody (bars = 50 μm) and (C) the number of F4/80-positive cells in WAT. (D) Frequency of CD45.1 and CD45.2 in ATMs of BM-WT and BM-KO mice. (E) Representative images of flow cytometry of ATMs fractionated by CD11b and F4/80 and (F) the number of $F4/80^{+}/CD11b^{+}$ cells in WAT. Values are expressed as mean ± standard error (n = 6 to 8). $^{*}p < 0.05$, $^{**}p < 0.01$, $^{***}p < 0.001$ vs. control diet group; $^{\#}p < 0.05$, $^{\#\#\#}p < 0.001$ vs. BM-WT group. CTL, control diet; HFD, high-fat diet; BM-WT mice, bone marrow wild-type chimeric mice; BM-KO mice, bone marrow ATRAP-deficient chimeric mice.

observed in BM-KO mice could be due to genetic alterations at the monocyte level. Transcriptome analysis of monocytes indicated that polarity to $CD206^{+}$ ATMs may be attenuated in monocytes derived from BM-KO mice. For example, CXCR2 is a chemokine receptor that promotes inflammation and is primarily expressed in neutrophils [28]. The finding that the deletion of CXCR2 promotes differentiation into $CD206^{+}$ ATMs suggests that the upregulation of CXCR2 in BM-KO mice is involved in suppressing the transition to $CD206^{+}$ ATMs [28]. Furthermore, gene cluster analysis showed that the HFD enhanced interferon response in monocytes of BM-KO mice. Interferon-γ is recognized as a potent proinflammatory activator of macrophages [41], and the enhancement of this response is also likely to prevent monocytes from shifting to $CD206^{+}$ ATMs in BM-KO mice. However, it should be noted that the sample size was small in these experiments, with N = 2 per group.

We previously reported that increased cardiovascular, kidney, and adipose tissue ATRAP expression improves pathological conditions, such as hypertension, diabetic kidney injury, and obesity [13,15,18,41,42]. Notably, in contrast to that in previous studies, the deletion of ATRAP in immune cells in the present study contributed to the amelioration of pathological changes related to visceral obesity. The systemic ATRAP-KO mice were presumably more affected by the obesity-exacerbating effect of ATRAP deficiency in adipose and other tissues, beyond the obesity-reducing effect resulting from the deficiency of ATRAP in immune cells. Importantly, this study revealed some of the functions of ATRAP in immune cells that had not been demonstrated in previous studies using systemic ATRAP-KO mice.

The strength of this study is that this is the first study to investigate the relationship between immune cell ATRAP and the pathogenesis of visceral obesity. We initially examined immune cell ATRAP expression in the early stage of obesity because it would be difficult to determine whether these changes were the cause or the result of the obesity pathology in the late phase investigation of obesity. The finding of increased immune cell ATRAP expression in the early stages of obesity, followed by improvement of obesity in bone marrow ATRAP-deficient mice, suggests that increased expression of immune cell ATRAP may be involved in the onset and progression of obesity, rather than being a consequence of the obesity pathology. In addition, leukocytes, including

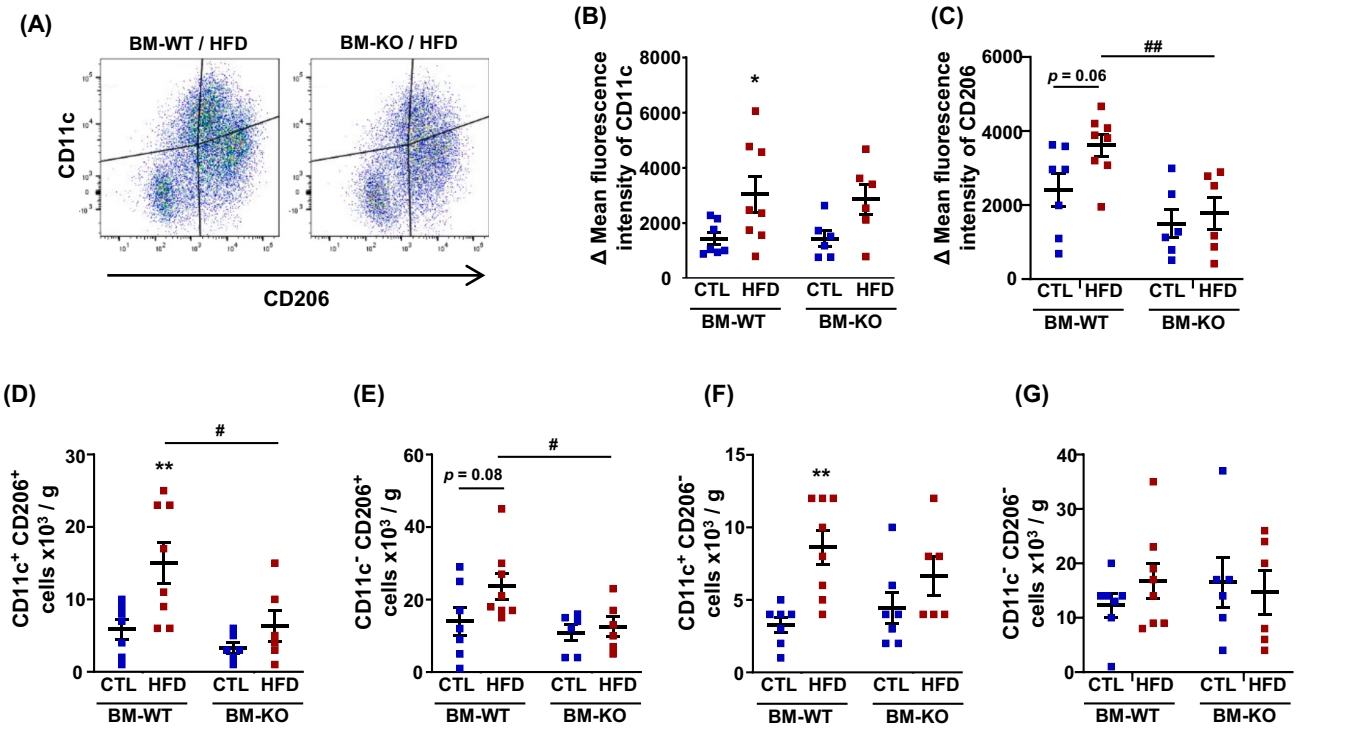

Fig. 7. Effect of bone marrow ATRAP deficiency on $CD11c^+$ and $CD206^+$ ATMs in HFD-induced obesity.
(A) Representative images of flow cytometry of ATMs fractionated by CD11c and CD206. Fluorescence intensity of (B) CD11c with anti-CD11c antibody and (C) CD206 staining with anti-CD206 antibody in ATMs fractionated by CD11b and F4/80. The number of (D) $CD11c^+/CD206^+$, (E) $CD11c^-/CD206^+$, (F) $CD11c^+/CD206^-$, and (G) $CD11c^-/CD206^-$ cells in WAT. Values are expressed as mean ± standard error (n = 6 to 8). $^*p < 0.05$, $^{**}p < 0.01$ vs. control diet group; $^{\#}p < 0.05$, $^{\#\#}p < 0.01$ vs. BM-WT group. CTL, control diet; HFD, high-fat diet; BM-WT mice, bone marrow wild-type chimeric mice; BM-KO mice, bone marrow ATRAP-deficient chimeric mice.

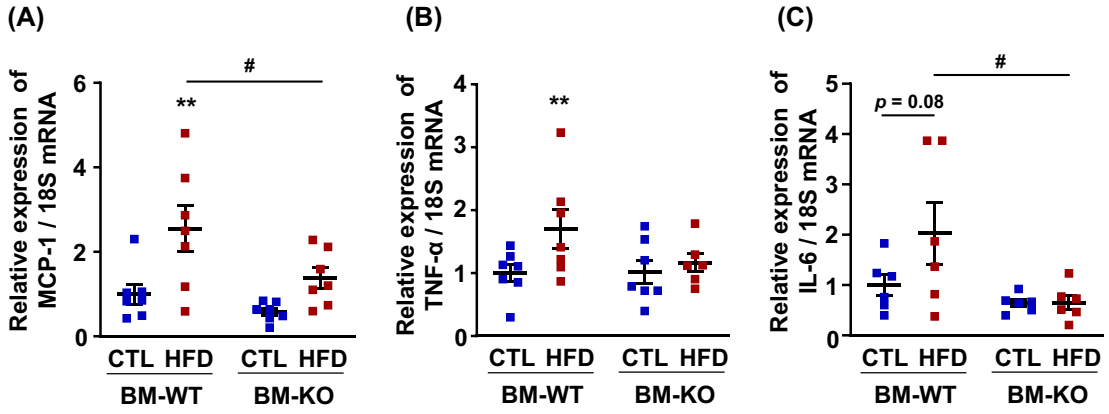

Fig. 8. Effect of bone marrow ATRAP deficiency on inflammation-related gene expression in WAT.
Relative mRNA expression of (A) MCP-1, (B) TNF-α, and (C) IL-6 in WAT. Values are expressed as mean ± standard error (n = 6 to 8). $^{**}p < 0.01$ vs. control diet group; $^{\#}p < 0.05$ vs. BM-WT group. CTL, control diet; HFD, high-fat diet; BM-WT mice, bone marrow wild-type chimeric mice; BM-KO mice, bone marrow ATRAP-deficient chimeric mice.

monocytes, can be tested by conventional blood drawing approach and may possibly be a more convenient biomarker or surrogate marker for visceral adipose obesity. Furthermore, in the present study, bone marrow ATRAP was found to be involved in the polarity of tissue macrophages. This finding has potential applications in other diseases. For example, the reduction in $CD206^+$ macrophage counts and suppression of downstream TGF-β signaling may lead to antifibrotic and anticancer effects [43–45]. However, the lack of evidence to prove their potential for practical use is still a weakness, and further studies are needed, especially including studies in humans.

This study has several limitations. First, the entire body was irradiated to generate BM-KO mice. This may have affected other organs, including adipose tissue. However, we do not have comparative data between bone marrow-transplanted and non-bone marrow-transplanted mice; therefore, it is not clear to what extent the effects of transplantation account for the results obtained in this study (including BM-WT and BM-KO mice). Second, we have no direct proof of the mechanism of inhibiting adipocyte hypertrophy, such as inhibition of TGF-β signaling. However, this aspect has been proven in several previous studies, and the results of this study are consistent with them. Third, other organs/tissues such as skeletal muscle, liver, and subcutaneous adipose tissue, which may affect metabolism in mice similar to

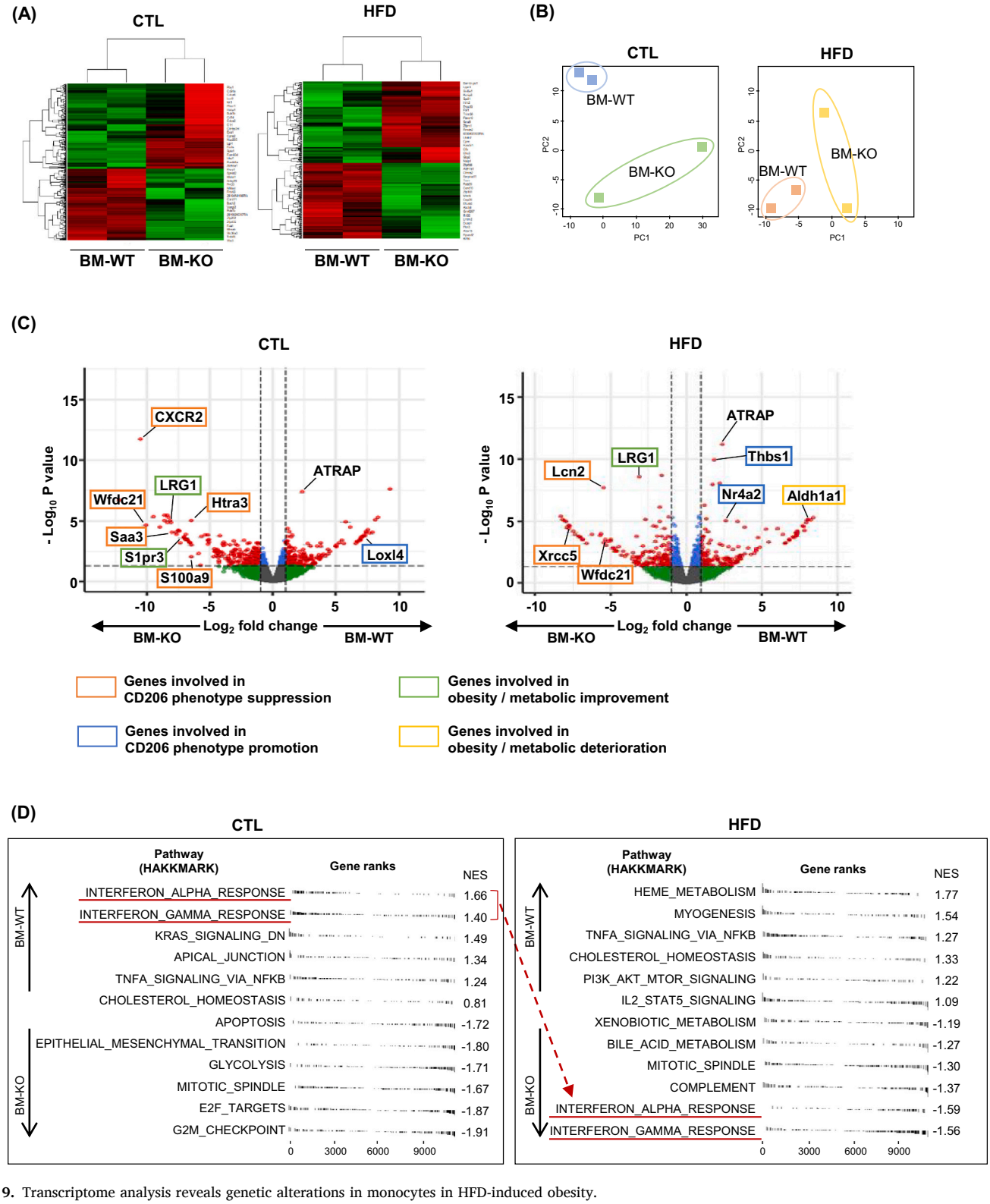

Fig. 9. Transcriptome analysis reveals genetic alterations in monocytes in HFD-induced obesity.
(A) Heatmaps of DEGs, (B) principal component analysis, and (C) volcano plots of RNA sequencing data derived from the monocytes of BM-WT and BM-KO mice fed a CTL or HFD for 8 weeks (n = 2 per group). (D) GSEA of DEGs that showed the enhancement of interferon-γ response in BM-KO mice fed an HFD. CTL, control diet; HFD, high-fat diet; BM-WT mice, bone marrow wild-type chimeric mice; BM-KO mice, bone marrow ATRAP-deficient chimeric mice.

visceral fat [46,47], were not fully investigated. In this study, the difference in the ITT slope was small compared to the reduction in visceral fat content. Immune cell ATRAP deficiency decreases HFD-induced visceral obesity, which should in itself, improve systemic metabolic parameters. On the other hand, it may also exacerbate insulin resistance in the liver and muscle, thus attenuating any positive systemic effects. In particular, the change in macrophage polarity (decrease in $CD206^{+}$ macrophages), which contributed to the anti-obesity effect of immune cell ATRAP deletion in this study, may increase tissue local inflammation and elicit insulin resistance in the liver and skeletal muscle [48,49].

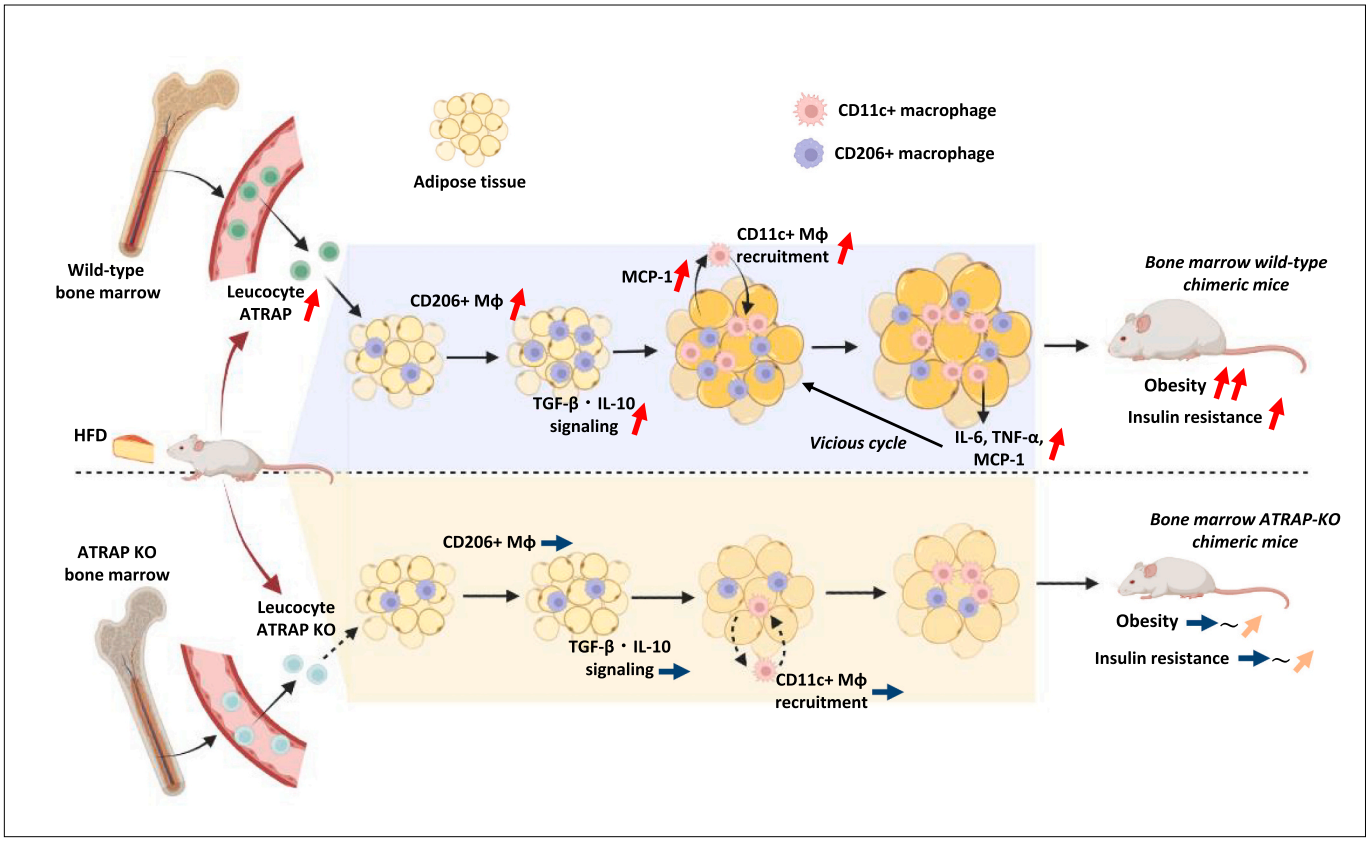

Fig. 10. Deficiency of bone marrow ATRAP exerts anti-obesity effects by inhibiting the increase in CD206$^+$ macrophage count and suppressing TGF-β and IL-10 signaling in white adipose tissue. Mφ, macrophage; HFD, high-fat diet.
The figure was created with "BioRender.com" and exported under a paid subscription, with an associated publication license.

However, these organs/tissues were not investigated in this study and require further study. Fourth, this study was performed using bone marrow transplantation; therefore, all immune cells may be involved in the phenotype. However, monocytes and macrophages were mainly analyzed in this study. Further analysis of other immune cells, such as neutrophils and lymphocytes, is required. Finally, energy metabolism was not evaluated. The lack of difference in caloric intake between the genotypes suggests increased energy expenditure in BM-KO/HFD mice. However, further investigation is needed to elucidate these mechanisms.

In conclusion, the upregulation of ATRAP expression in immune cells from the early stages of obesity leads to a shift in polarity toward CD206$^+$ macrophages in adipose tissue, thus promoting visceral fat accumulation and visceral obesity. This, in turn, contributes to the pathogenesis of impaired glucose tolerance and insulin resistance as a phenotypic change to metabolic disorders. Our results suggest that modulation of ATRAP expression in immune cells may affect visceral adipose obesity and related metabolic disorders and may serve as a biomarker for obesity pathogenesis, but further studies are needed.

Funding

This work was supported by the Yokohama Foundation for Advancement of Medical Science, Uehara Memorial Foundation, Japan Society for the Promotion of Science, Japan Kidney Association-Nippon Boehringer Ingelheim Joint Research Program, Japanese Association of Dialysis Physicians, Strategic Research Project of Yokohama City University, Moriya Scholarship Foundation, Salt Science Research Foundation, Bayer Scholarship for Cardiovascular Research, Mochida Memorial Foundation for Medical and Pharmaceutical Research, and Yokohama City University (for a grant under the "KAMOME Project").

CRediT authorship contribution statement

Research conception and study design: SHU.T., T.S., H.W., and H.O.; data acquisition: SHU.T., T.S., and J.I.; data analysis/interpretation: SHU.T., T.S., T.U., J.I., and H.O.; statistical analysis: SHU.T., T.S., H.W., and K.A.; writing of the manuscript: SHU.T., T.S., H.W., T.U., J.I., H.O., K.H., K.A., E.A, SHO.T, SHI.T, K.H., S.K., A.Y., T.T., and K.T.; supervision or mentorship: H.W., K.A., T.T., and K.T. All authors contributed important intellectual content during the drafting and revision of the manuscript. They agree to be personally accountable for their contributions and to ensure that questions about the accuracy or integrity of any portion of the work (even if they were not directly involved) were appropriately investigated and resolved, with documentation if appropriate.

Declaration of competing interest

The authors declare that they have no known competing financial interests or personal relationships that could have appeared to influence the work reported in this paper.

Data availability

Data from this work will be shared upon reasonable request to the corresponding author.

The accession number of RNA-seq data is DRA016279 (DRA in DDBJ).

Acknowledgments

We would like to thank A. Kuwae (Yokohama City University), E.

Maeda (Yokohama City University), and K. Aoyagi (Yokohama City University) for their help with the experiments. We would also like to thank the MEXT Joint Usage/Research Center Program at the Advanced Medical Research Center, Yokohama City University, for providing bioinformatics educational programs, which helped us to perform data analyses in this study. Lastly, we would like to thank Editage (www.editage.com) for English language editing.

Appendix A. Supplementary data

Supplementary data to this article can be found online at https://doi.org/10.1016/j.metabol.2023.155706.

References

[1] Trends in adult body-mass index in 200 countries from 1975 to 2014: a pooled analysis of 1698 population-based measurement studies with 19·2 million participants. Lancet 2016;(387):1377–96.
[2] Blüher M, Aras M, Aronne LJ, Batterham RL, Giorgino F, Ji L, et al. New insights into the treatment of obesity. Diabetes Obes Metab 2023;25:2058–72.
[3] Afshin A, Forouzanfar MH, Reitsma MB, Sur P, Estep K, Lee A, et al. Health effects of overweight and obesity in 195 countries over 25 years. N Engl J Med 2017;377:13–27.
[4] Chintam K, Chang AR. Strategies to treat obesity in patients with CKD. Am J Kidney Dis 2021;77:427–39.
[5] Hill MA, Yang Y, Zhang L, Sun Z, Jia G, Parrish AR, et al. Insulin resistance, cardiovascular stiffening and cardiovascular disease. Metabolism 2021;119:154766.
[6] Larsson SC, Spyrou N, Mantzoros CS. Body fatness associations with cancer: evidence from recent epidemiological studies and future directions. Metabolism 2022;137:155326.
[7] Jo J, Gavrilova O, Pack S, Jou W, Mullen S, Sumner AE, et al. Hypertrophy and/or hyperplasia: dynamics of adipose tissue growth. PLoS Comput Biol 2009;5:e1000324.
[8] Stenkula KG, Erlanson-Albertsson C. Adipose cell size: importance in health and disease. Am J Physiol Regul Integr Comp Physiol 2018;315:R284–r95.
[9] Odegaard JI, Chawla A. Alternative macrophage activation and metabolism. Annu Rev Pathol 2011;6:275–97.
[10] Nawaz A, Aminuddin A, Kado T, Takikawa A, Yamamoto S, Tsuneyama K, et al. CD206(+) M2-like macrophages regulate systemic glucose metabolism by inhibiting proliferation of adipocyte progenitors. Nat Commun 2017;8:286.
[11] Oliveira MC, Silveira ALM, de Oliveira ACC, Lana JP, Costa KA, Vieira ÉLM, et al. Eosinophils protect from metabolic alterations triggered by obesity. Metabolism 2023;146:155613.
[12] Tamura K, Azushima K, Kinguchi S, Wakui H, Yamaji T. ATRAP, a receptor-interacting modulator of kidney physiology, as a novel player in blood pressure and beyond. Hypertens Res 2022;45:32–9.
[13] Haruhara K, Suzuki T, Wakui H, Azushima K, Kurotaki D, Kawase W, et al. Deficiency of the kidney tubular angiotensin II type1 receptor-associated protein ATRAP exacerbates streptozotocin-induced diabetic glomerular injury via reducing protective macrophage polarization. Kidney Int 2022;101:912–28.
[14] Wakui H, Uneda K, Tamura K, Ohsawa M, Azushima K, Kobayashi R, et al. Renal tubule angiotensin II type 1 receptor-associated protein promotes natriuresis and inhibits salt-sensitive blood pressure elevation. J Am Heart Assoc 2015;4:e001594.
[15] Azushima K, Ohki K, Wakui H, Uneda K, Haku S, Kobayashi R, et al. Adipocyte-specific enhancement of angiotensin II type 1 receptor-associated protein ameliorates diet-induced visceral obesity and insulin resistance. J Am Heart Assoc 2017:6.
[16] Ohsawa M, Tamura K, Wakui H, Maeda A, Dejima T, Kanaoka T, et al. Deletion of the angiotensin II type 1 receptor-associated protein enhances renal sodium reabsorption and exacerbates angiotensin II-mediated hypertension. Kidney Int 2014;86:570–81.
[17] Haruhara K, Wakui H, Azushima K, Kurotaki D, Kawase W, Uneda K, et al. Angiotensin receptor-binding molecule in leukocytes in association with the systemic and leukocyte inflammatory profile. Atherosclerosis 2018;269:236–44.
[18] Kobayashi R, Wakui H, Azushima K, Uneda K, Haku S, Ohki K, et al. An angiotensin II type 1 receptor binding molecule has a critical role in hypertension in a chronic kidney disease model. Kidney Int 2017;91:1115–25.
[19] Pedro PF, Tsakmaki A, Bewick GA. The glucose tolerance test in mice. Methods Mol Biol 2020;2128:207–16.
[20] Matsumoto K, Miyake S, Yano M, Ueki Y, Yamaguchi Y, Akazawa S, et al. Insulin resistance and arteriosclerosis obliterans in patients with NIDDM. Diabetes Care 1997;20:1738–43.
[21] Matthews DR, Hosker JP, Rudenski AS, Naylor BA, Treacher DF, Turner RC. Homeostasis model assessment: insulin resistance and beta-cell function from fasting plasma glucose and insulin concentrations in man. Diabetologia 1985;28:412–9.
[22] Tsukamoto S, Wakui H, Azushima K, Yamaji T, Urate S, Suzuki T, et al. Tissue-specific expression of the SARS-CoV-2 receptor, angiotensin-converting enzyme 2, in mouse models of chronic kidney disease. Sci Rep 2021;11:16843.
[23] Subramanian A, Tamayo P, Mootha VK, Mukherjee S, Ebert BL, Gillette MA, et al. Gene set enrichment analysis: a knowledge-based approach for interpreting genome-wide expression profiles. Proc Natl Acad Sci U S A 2005;102:15545–50.
[24] Yadav H, Quijano C, Kamaraju AK, Gavrilova O, Malek R, Chen W, et al. Protection from obesity and diabetes by blockade of TGF-β/Smad3 signaling. Cell Metab 2011;14:67–79.
[25] Deng R, Li C, Wang X, Chang L, Ni S, Zhang W, et al. Periosteal CD68(+) F4/80(+) macrophages are mechanosensitive for cortical bone formation by secretion and activation of TGF-β1. Adv Sci (Weinh) 2022;9:e2103343.
[26] Mahajan S, Saini A, Chandra V, Nanduri R, Kalra R, Bhagyaraj E, et al. Nuclear receptor Nr4a2 promotes alternative polarization of macrophages and confers protection in sepsis. J Biol Chem 2015;290:18304–14.
[27] Busnadiego O, González-Santamaría J, Lagares D, Guinea-Viniegra J, Pichol-Thievend C, Muller L, et al. LOXL4 is induced by transforming growth factor β1 through Smad and JunB/Fra2 and contributes to vascular matrix remodeling. Mol Cell Biol 2013;33:2388–401.
[28] Dyer DP, Pallas K, Medina-Ruiz L, Schuette F, Wilson GJ, Graham GJ. CXCR2 deficient mice display macrophage-dependent exaggerated acute inflammatory responses. Sci Rep 2017;7:42681.
[29] Ko T, Nomura S, Yamada S, Fujita K, Fujita T, Satoh M, et al. Cardiac fibroblasts regulate the development of heart failure via Htra3-TGF-β-IGFBP7 axis. Nat Commun 2022;13:3275.
[30] Chait A, Wang S, Goodspeed L, Gomes D, Turk KE, Wietecha T, et al. Sexually dimorphic relationships among Saa3 (serum amyloid A3), inflammation, and cholesterol metabolism modulate atherosclerosis in mice. Arterioscler Thromb Vasc Biol 2021;41:e299–313.
[31] Xie Z, Guo Z, Liu J. Whey acidic protein/four-disulfide core domain 21 regulate sepsis pathogenesis in a mouse model and a macrophage cell line via the Stat3/Toll-like receptor 4 (TLR4) signaling pathway. Med Sci Monit 2018;24:4054–63.
[32] Sun H, Li Q, Yin G, Ding X, Xie J. Ku70 and Ku80 participate in LPS-induced pro-inflammatory cytokines production in human macrophages and monocytes. Aging (Albany NY) 2020;12:20432–44.
[33] Shibata K, Sato K, Shirai R, Seki T, Okano T, Yamashita T, et al. Lipocalin-2 exerts pro-atherosclerotic effects as evidenced by in vitro and in vivo experiments. Heart Vessels 2020;35:1012–24.
[34] Franz S, Ertel A, Engel KM, Simon JC, Saalbach A. Overexpression of S100A9 in obesity impairs macrophage differentiation via TLR4-NFkB-signaling worsening inflammation and wound healing. Theranostics 2022;12:1659–82.
[35] Choi CHJ, Barr W, Zaman S, Model C, Park A, Koenen M, et al. LRG1 is an adipokine that promotes insulin sensitivity and suppresses inflammation. Elife 2022:11.
[36] Chakrabarty S, Bui Q, Badeanlou L, Hester K, Chun J, Ruf W, et al. S1P/S1PR3 signalling axis protects against obesity-induced metabolic dysfunction. Adipocyte 2022;11:69–83.
[37] Vijayachandra K, Higgins W, Lee J, Glick A. Induction of p16ink4a and p19ARF by TGFbeta1 contributes to growth arrest and senescence response in mouse keratinocytes. Mol Carcinog 2009;48:181–6.
[38] Yamazaki S, Ema H, Karlsson G, Yamaguchi T, Miyoshi H, Shioda S, et al. Nonmyelinating Schwann cells maintain hematopoietic stem cell hibernation in the bone marrow niche. Cell 2011;147:1146–58.
[39] Rajbhandari P, Thomas BJ, Feng AC, Hong C, Wang J, Vergnes L, et al. IL-10 signaling remodels adipose chromatin architecture to limit thermogenesis and energy expenditure. Cell 2018;172:218–33 (e17).
[40] Nour J, Moregola A, Svecla M, Da Dalt L, Bellini R, Neyrolles O, et al. Mannose receptor deficiency impacts bone marrow and circulating immune cells during high fat diet induced obesity. Metabolites 2022:12.
[41] Ivashkiv LB. IFNγ: signalling, epigenetics and roles in immunity, metabolism, disease and cancer immunotherapy. Nat Rev Immunol 2018;18:545–58.
[42] Wakui H, Tamura K, Masuda S, Tsurumi-Ikeya Y, Fujita M, Maeda A, et al. Enhanced angiotensin receptor-associated protein in renal tubule suppresses angiotensin-dependent hypertension. Hypertension 2013;61:1203–10.
[43] Tang PM, Nikolic-Paterson DJ, Lan HY. Macrophages: versatile players in renal inflammation and fibrosis. Nat Rev Nephrol 2019;15:144–58.
[44] Peng D, Fu M, Wang M, Wei Y, Wei X. Targeting TGF-β signal transduction for fibrosis and cancer therapy. Mol Cancer 2022;21:104.
[45] Debacker JM, Gondry O, Lahoutte T, Keyaerts M, Huvenne W. The prognostic value of CD206 in solid malignancies: a systematic review and meta-analysis. Cancers (Basel) 2021:13.
[46] Mastrototaro L, Roden M. Insulin resistance and insulin sensitizing agents. Metabolism 2021;125:154892.
[47] Kahn DE, Bergman BC. Keeping it local in metabolic disease: adipose tissue paracrine signaling and insulin resistance. Diabetes 2022;71:599–609.
[48] Olefsky JM, Glass CK. Macrophages, inflammation, and insulin resistance. Annu Rev Physiol 2010;72:219–46.
[49] Li C, Xu MM, Wang K, Adler AJ, Vella AT, Zhou B. Macrophage polarization and meta-inflammation. Transl Res 2018;191:29–44.